Revised version submitted to ApJ
Preprint typeset using LaTeX style emulateapj v. 10/09/06

CALIBRATION OF THE MASS–TEMPERATURE RELATION FOR CLUSTERS OF GALAXIES USING WEAK GRAVITATIONAL LENSING[1]

Kristian Pedersen
Dark Cosmology Centre, Niels Bohr Institute, University of Copenhagen, Juliane Maries Vej 30, DK-2100, Copenhagen Ø, Denmark

Håkon Dahle[2]
Institute of Theoretical Astrophysics, University of Oslo, P.O. Box 1029, Blindern, N-0315 Oslo, Norway
Revised version submitted to ApJ

ABSTRACT

The main uncertainty in current determinations of the power spectrum normalization, σ_8, from abundances of X-ray luminous galaxy clusters arises from the calibration of the mass–temperature relation. We use our weak lensing mass determinations of 30 clusters from the hitherto largest sample of clusters with lensing masses, combined with X-ray temperature data from the literature, to calibrate the normalization of this relation at a temperature of 8 keV, $M_{500c,8keV} = (8.7 \pm 1.6)\,h^{-1}\,10^{14} M_\odot$. This normalization is consistent with previous lensing-based results based on smaller cluster samples, and with some predictions from numerical simulations, but higher than most normalizations based on X-ray derived cluster masses. Assuming the theoretically expected slope $\alpha = 3/2$ of the mass–temperature relation, we derive $\sigma_8 = 0.88 \pm 0.09$ for a spatially-flat ΛCDM universe with $\Omega_m = 0.3$. The main systematic errors on the lensing masses result from extrapolating the cluster masses beyond the field-of-view used for the gravitational lensing measurements, and from the separation of cluster/background galaxies, contributing each with a scatter of 20%. Taking this into account, there is still significant intrinsic scatter in the mass–temperature relation indicating that this relation may not be very tight, at least at the high mass end. Furthermore, we find that dynamically relaxed clusters are 75 ± 40% hotter than non-relaxed clusters.

Subject headings: Cosmology: observations — cosmological parameters — dark matter — gravitational lensing — Galaxies: clusters

1. INTRODUCTION

The abundance of massive clusters of galaxies provides sensitive constraints on the cosmological parameters that govern structure growth in the universe. However, a prerequisite for this is reliable mass measurements for large samples of clusters with well-understood selection criteria. Cluster mass measurements used have traditionally come from virial analysis of the velocity dispersion measurements of cluster galaxies (e.g., Frenk et al. 1990; Carlberg et al. 1997; Borgani et al. 1999), or X-ray temperature measurements of the hot intracluster gas under the assumption that the gas is in hydrostatic equilibrium (for a review see Rosati, Borgani & Norman 2002). Satellite observatories such as ROSAT, ASCA, XMM-Newton and *Chandra* have made increasingly accurate X-ray temperature measurements of clusters, and have produced well-defined cluster samples of sufficient size to accurately measure the X-ray temperature and luminosity functions (e.g. Henry 2004; Böhringer et al. 2002). However, the relation between cluster mass and X-ray temperature and luminosity, respectively, must be determined to convert these into a reliable cluster mass function.

X-ray luminosities are available for large samples of clusters, but the X-ray luminosity is highly sensitive to the complex physics of cluster cores, making it challenging to relate to cluster mass. Measuring X-ray temperatures is observationally much more demanding, but the X-ray temperature is mainly determined by gravitational processes and is hence more directly related to cluster mass than X-ray luminosity. Both from simulations and observations the intrinsic scatter in mass around the mass–temperature relation is thus found to be much smaller ($\Delta M/M \approx 0.15$, Evrard, Metzler, & Navarro 1996; Borgani et al. 2004; Sanderson et al. 2003; Vikhlinin et al. 2006) than the scatter in mass around the mass–luminosity relation ($\Delta M/M \approx 0.4$, Reiprich & Böhringer 2002).

Two different routes have been followed for determining the mass–temperature relation. Most studies have used a small sample (up to about a dozen) of supposedly well understood clusters for which the assumptions underlying the mass determination should be fulfilled to a high degree. The main concern for this approach is that the selected clusters may not be representative of the whole cluster population, and therefore the derived mass–temperature relation may only apply to a subset of clusters. Alternatively, the mass–temperature relation may be determined from a large sample of more objectively selected clusters. This is more fruitful when comparing such a locally determined mass–temperature relation to a sample of high-redshift clusters where the data quality does not allow a similar selection of the "most suitable" clusters. Also, mass–temperature relations derived from simulations are usually based on a large range of simulated clusters with no pre-selection. Hence it is most appropriate to compare observationally obtained mass–temperature relations determined from all available clusters to the relations from simulations. On the other hand, for some of the clusters in such a sample the hydrostatic assumption may be invalid, making X-ray based mass determinations unreliable for a subset of the clusters. A larger scatter (which may not be symmetric) around the mean mass–temperature relation may be expected, when such clusters are included.

Electronic address: kp@dark-cosmology.dk
Electronic address: hdahle@astro.uio.no

[1] Based on observations made with the Nordic Optical Telescope, operated on the island of La Palma jointly by Denmark, Finland, Iceland, Norway, and Sweden, in the Spanish Observatorio del Roque de los Muchachos of the Instituto de Astrofísica de Canarias

[2] Visiting observer, University of Hawaii 2.24m Telescope at Mauna Kea Observatory, Institute for Astronomy, University of Hawaii

There are still poorly understood systematic uncertainties associated with establishing the mass–temperature relation. The normalization of the mass–temperature relation based on cluster masses determined from X-ray data (Finoguenov, Reiprich, & Böhringer 2001; Vikhlinin et al. 2006; Arnaud, Pointecouteau, & Pratt 2005), tend to differ significantly between studies, and from the expectations based on numerical simulations (e.g., Evrard et al. 1996; Eke et al. 1998; Pen 1998; Borgani et al. 2004). The determination of this normalization is currently the dominating source of discrepancies between the reported values for the power spectrum normalization on the scale of galaxy clusters, σ_8, derived from the observed cluster temperature function (Huterer & White 2002; Seljak 2002; Pierpaoli et al. 2003; Henry 2004). Observations using X-ray based mass determinations have traditionally favored low normalizations (and hence low values of σ_8), while simulations have favored somewhat higher normalizations.

Gravitational lensing provides an opportunity to measure cluster masses without invoking the assumption of hydrostatic equilibrium in the hot intra-cluster gas implicit in the X-ray based mass determinations. Also, in this case the measurement of cluster mass is truly independent of the X-ray temperature measurement. Hjorth, Oukbir & van Kampen (1998) used weak gravitational mass measurements for eight clusters drawn from the literature to find a relation between mass over cluster-centric radius, and temperature. They determined a normalization of this relation consistent with the value predicted by Evrard et al. (1996), but with a preference for somewhat higher cluster masses (if the redshift scaling of equation 5 is assumed, see below). However, Smith et al. (2005; hereafter S05) determined a mass–temperature relation with a normalization significantly lower than indicated by the Hjorth et al. (1998) study. S05 based their results on a sample of 10 clusters with weak lensing masses and temperatures determined from *Chandra* data.

Here, we present a new weak gravitational lensing-based measurement of the normalization of the mass–temperature relation. The main improvements with respect to the work of Hjorth et al. (1998) and S05 is that we use a significantly larger cluster sample which represents a significant fraction of all the clusters in an even larger sample with well-defined objective selection criteria (Dahle et al. 2002; H. Dahle 2006, in preparation). An additional improvement over the work of Hjorth et al. (1998) is that the weak lensing analysis has been performed in a consistent way for all clusters, using the same shear estimator and making the same assumptions about e.g., the typical redshift of the lensed galaxy population and the degree of contamination by cluster galaxies. We note that the early data set of clusters with published weak lensing masses used by Hjorth et al. (1998) is biased at some level towards systems that were observed because of "extreme" properties, such as being the hottest or most X-ray luminous system known at the time, or having a large number of strongly gravitationally lensed arcs. Furthermore, we note that our gravitational lensing measurements are made at larger radii than probed by S05, requiring smaller extrapolations to estimate the mass within e.g., the virial radii of the clusters.

The data set used for the analysis is described in § 2, our results for the mass–temperature relation and σ_8 are presented in § 3, and our results are compared to other work and the implications discussed in § 4.

Except when specifically noted otherwise (for easy comparison to previous results using different cosmologies), we assume a spatially–flat cosmology with a cosmological constant ($\Omega_m = 0.3$, $\Omega_\Lambda = 0.7$), and the Hubble parameter is given by $H_0 = 100h\,\mathrm{km\,s^{-1}Mpc^{-1}}$.

2. DATA SET

2.1. *Weak lensing data*

Our weak lensing data set is a sample of 30 clusters (see Table 1), of which 28 were included in the weak lensing cluster sample of Dahle et al. (2002). Data for two additional clusters come from a recent extension of this data set (H. Dahle 2006, in preparation). The clusters targeted for these weak lensing studies were generally selected to lie above an X-ray luminosity limit $L_{X,0.1-2.4\,\mathrm{keV}} \geq 6\times10^{44}$ ergs s^{-1} (this luminosity limit is for our chosen cosmology with $h = 0.7$) and within a redshift range $0.15 < z_{\mathrm{cl}} < 0.35$. The observed clusters were selected from the X-ray luminous cluster samples of Briel & Henry (1993) and Ebeling et al. (1996;1998;2000). The cluster samples of the first two of these papers are based on correlating an optically selected cluster sample (Abell 1958; Abell, Corwin, & Olowin 1989) with X-ray sources from the ROSAT All-Sky Survey (RASS; Trümper et al. 1993), while the two last papers contain X-ray flux limited cluster catalogs, also based on RASS. Of the total sample of 30 clusters, three (A959, A1722, and A1995) are drawn from the Briel & Henry (1993) sample and two (A209 and A2104) are drawn from the XBAC sample of Ebeling et al. (1996). Of the remaining 25 clusters, 22 are included in the X-ray brightest cluster sample (BCS) of Ebeling et al. (1998), while three (A611, A1576, and Zw3146) come from its low-flux extension (eBCS; Ebeling et al. 2000). Of the BCS and eBCS clusters in our sample, 24 objects are included in a volume-limited sample of 35 clusters selected from the BCS and eBCS samples (Dahle 2006). Hence, while our sample is not strictly physically well-defined (in the sense that the availability of an X-ray temperature measurement is one of the defining selection criteria), it still has significant overlap with a well-defined cluster sample. In a recent paper, Stanek et al. (2006) discuss how a significant scatter around the mean mass-luminosity relation may cause a significant Malmquist bias in X-ray flux-limited cluster samples, causing high-mass, low flux clusters to drop out at high redshifts. This would result in a bias in the mass-luminosity (or mass-temperature) relation derived based on such a sample. We note, however, that although the RASS-based samples from which our cluster sample is drawn are flux-limited, the cluster sample discussed here quite closely approximates a volume-limited sample, and we therefore expect any such bias to be negligible.

The observations were made with the 8192^2 UH8K mosaic CCD camera and the 2048^2 Tek CCD camera at the 2.24m University of Hawaii Telescope and with the 2048^2 ALFOSC CCD camera at the 2.56m Nordic Optical Telescope. All clusters were imaged in both the *I*- and *V*-band, with typical total exposure times of 3.5h in each passband for the UH8K data and $\sim$ 1.5h for the data obtained with the more sensitive 2048^2 detectors. The seeing was in the range $0\farcs6 \leq \mathrm{FWHM} \leq 1\farcs1$ for all the imaging data used for the weak lensing analysis. The median seeing was $0\farcs82$ in the *I*-band and $0\farcs9$ in the *V*-band. This gave typically $\sim$ 25 usable background galaxies per square arcminute, or a "figure of merit" value of $\sum Q^2/d\Omega \simeq 1.5\times10^5\mathrm{deg}^{-2}$, as defined by Kaiser (2000). As noted below, the background galaxies were selected based

on signal to noise ratio rather than magnitude, with limits corresponding to $21 \lesssim m_I \lesssim 24.5$ and $22 \lesssim m_V \lesssim 25.5$ for point sources. The observations and data reduction of the data set used for the weak lensing mass measurements are described in detail by Dahle et al. (2002).

Major efforts are being made to improve the methods for the estimation of weak gravitational lensing, particularly in connection with ongoing and future studies of "cosmic shear" based on wide-field optical surveys. The requirements for the precision of shear estimates in these surveys are substantially more stringent than for weak lensing observations of massive clusters, given the significantly weaker lensing effects measured in random fields.

In this work, we have used the shear estimator of Kaiser (2000), which was "blind-tested" (along with several other shear estimators) by Heymans et al. (2005), using simulated lensing data. The shear estimator of Kaiser (2000) is more mathematically rigorous than the currently most widely used shear estimator (Kaiser, Squires, & Broadhurst 1995), but it displays a significant non-linear response to shear, unlike most other shear estimators. If we correct our shear values using a second order polynomial based on the test results of Heymans et al. (2005), we find that most cluster masses stay within $+/-15\%$ of the mass calculated based on uncorrected shear values. Furthermore, the change in average cluster mass is $< 2\%$, i.e., there is very little systematic shift in mass. In the end, we chose not to apply this correction, since it would, in a few cases, require extrapolations outside the range of shear values over which the shear estimator has been tested. For more details about the practical implementation of this shear estimator, see Dahle et al. (2002).

To convert the measurements of weak gravitational shear into actual cluster masses, the distances to the background galaxies need to be known. The background galaxy redshifts were estimated from spectroscopic and photometric redshifts in the Hubble Deep Field (for details, see Dahle et al. 2002). For our data set and chosen cosmological model, the average value of the ratio between the lens-source and observer-source angular diameter distances, $\beta \equiv D_{ls}/D_s$, is well approximated by the relation $\langle\beta\rangle = 1.37 z_{\rm cl}^2 - 2.00 z_{\rm cl} + 1.01$ within the redshift range of our cluster sample. This then provides an effective critical surface density for lensing ($\Sigma_{\rm crit} = (c^2/4\pi G)(D_l\langle\beta\rangle)^{-1}$; where D_l is the angular diameter distance to the cluster), which is used for deriving cluster masses from the shear estimates. The quoted value of $\langle\beta\rangle$ corresponds to the value at large cluster radii; at smaller radii a correction term has to be employed to account for contamination by cluster galaxies, as discussed below and illustrated in Figure 1.

The observable galaxy shape distortions caused by gravitational lensing provide a measurement of the reduced tangential shear, $g_T = \gamma_T/(1-\kappa)$, where γ_T is the tangential component of the shear and κ is the convergence. We fit an NFW-type mass density profile,

$$\rho(r) = \frac{\delta_c \rho_c(z)}{(r/r_s)(1+r/r_s)^2} \qquad (1)$$

(Navarro, Frenk, & White 1997), to the observed reduced shear profile $g_T(r)$ of each cluster. Here, $\rho_c(z)$ is the critical density of the universe at the redshift of the cluster, and

$$\delta_c = \frac{200}{3}\frac{c_{200}^3}{\ln(1+c_{200}) - c_{200}/(1+c_{200})}. \qquad (2)$$

We assumed a concentration parameter $c_{200} = c_{\rm vir}/1.194 = 4.9/(1+z)$, corresponding to the median halo concentration predicted by Bullock et al. (2001) for a $M_{\rm vir} \simeq 8\times10^{14} M_\odot$ cluster from simulations of dark matter halos in a ΛCDM universe. Here, $c_{200} = r_{200c}/r_s$, and $c_{\rm vir} = r_{\rm vir}/r_s$, where r_{200c} is defined as the radius within which the average mass density is 200 times the critical density $\rho_c(z)$, and $r_{\rm vir}$ is the virial radius of the cluster.

The lensing properties of the NFW model have been calculated by Bartelmann (1996) and Wright & Brainerd (2000). From our fit, we calculated M_{500c}, the mass enclosed by the radius r_{500c}. The mass estimates are listed in Table 1. The shear measurements used for the fit were made at clustercentric radii $50'' < r < 180''$ for the clusters that were observed with 2048^2 CCD cameras and $150'' < r < 550''$ for the clusters that were observed with the UH8K camera. By comparison, we find r_{500c} values typically in the range $300'' < r_{500c} < 600''$ for the clusters we study here. In many cases, we need to extrapolate the NFW profile out to r_{500c} (in Table 1 we list the ratio of the outermost radii of our shear measurements, $r_{\rm fit}$, to r_{500c}, and note that $r_{500c} = 0.66 r_{200c}$ for our chosen NFW model). In this extrapolation, we assume the median NFW concentration parameter given above. Hence, any intrinsic scatter in $c_{\rm vir}$ will introduce an extra uncertainty in the cluster mass estimates. If we assume a random scatter around the mean value of $c_{\rm vir}$ at the level (a 1σ $\Delta(\log c_{\rm vir}) \sim 0.18$) predicted by Bullock et al. (2001), we find a corresponding scatter in the mass estimates of 20% for our data set. This additional scatter is not included in the uncertainties of the listed mass measurements in Table 1, but is considered further in Section 3.2.

The measured gravitational lensing signal is sensitive to the two-dimensional surface mass distribution, including mass associated with the cluster outside r_{500c}, and random structures seen in projection along the line of sight (Metzler, White & Loken 2001; Hoekstra 2001; Clowe, De Lucia & King 2004; de Putter & White 2005). This will introduce additional uncertainty (and potentially a net bias) to any lensing-based estimates of the cluster mass contained within a 3D volume. Studies based on simulated clusters (e.g., Clowe et al. 2004) indicate that the net bias is no more than a few percent when 3D cluster masses are estimated by fitting observations of $g_T(r)$ to predictions from theoretical models of the mass distribution, such as the NFW model. However, the scatter in the mass estimates from projection effects amount to a weak lensing mass dispersion of $\sim 15-25\%$ for massive galaxy clusters, which should be added to the observational uncertainties of the lensing mass estimates. In this paper, we have assumed a lensing mass dispersion of 0.26 resulting from projection effects, corresponding to the value estimated by Metzler, White & Loken (2001) from their N-body simulations. Although these authors considered a somewhat different mass estimator, more recent estimates indicate a similar mass dispersion for the NFW profile fitting method that we have used. This additional mass uncertainty has been added in quadrature to the uncertainties of M_{500c} values listed in Table 1.

The absence of reliable information about the individual redshifts of the faint galaxies used for the weak lensing measurement will inevitably result in some degree of confusion between lensed background galaxies and unlensed cluster galaxies. The magnitude of this effect will depend on the projected number density of cluster galaxies, and should thus have a strong dependency on cluster radius. Hence, a radially dependent correction factor was applied to the shear measurements to correct for contamination from cluster galax-

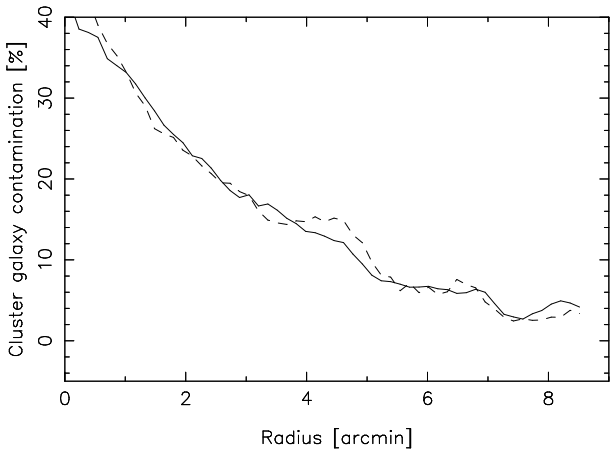

FIG. 1.— Cluster galaxy contamination in the faint galaxy catalogs as a function of distance from the cluster center. The solid line represents an average of 6 clusters at an average redshift $\langle z \rangle = 0.31$, while the dashed line represents an average of 5 clusters at $\langle z \rangle = 0.23$.

ies in the faint galaxy catalogs that were used to measure the gravitational shear (these catalogs included all galaxies in the cluster fields that were detected at a signal-to-noise ratio $6 < S/N < 100$, with no additional selection based on e.g., galaxy color). The magnitude of this correction was estimated from the radial dependence of the average faint galaxy density in two "stacks" of clusters observed with the UH8K camera, one at $z \sim 0.30$ and the other at $z \sim 0.23$, assuming that the contamination is negligible at the edge of the UH8K fields, $> 1.5h^{-1}$ Mpc from the cluster center. The estimated degree of contamination is shown in Figure 1.

Given the difference in cluster redshift, the similarity of the two curves in Figure 1 may be somewhat surprising, as one would naively expect the more distant clusters to display a significantly lower surface density of cluster galaxies. However, there are several competing effects that affect the observed galaxy density at a fixed angular radius: Firstly, if all cluster galaxies were detectable regardless of cluster redshift, the change in apparent image scale with redshift should increase the surface density by a factor given by the square of the ratio of the angular diameter distances. On the other hand, a fixed angular radius would correspond to a larger physical cluster-centric radius (and hence lower galaxy density in physical units) at the larger redshift, the difference depending on the slope of the radial galaxy density profile. At the radii probed in this study, both the radial surface mass density profile and the number density profile of bright cluster galaxies follow approximately the power law behavior of a singular isothermal sphere ($\sigma(r) \propto r^a$, with $a = -1$). Hence, the physical number density (in galaxies/Mpc^2) at a fixed angular radius should decrease as the inverse of the ratio of angular diameter distances. In addition, the faintest galaxies drop below the detection limit at higher redshift, the effect depending on the slope of the cluster luminosity function around $M_R \approx -15$. Assuming a Schechter (1976) luminosity function with a faint-end slope $\alpha^\star = -1.25$ (typical of rich clusters) and $M_R^\star(z = 0.23) = -21.65$, the luminosity function can be integrated down to the detection limit (corresponding to $M_R \simeq -15.0$ and $M_R \simeq -15.7$ at $z = 0.23$ and $z = 0.30$, respectively), to estimate the fraction of cluster galaxies that drop out at the higher redshift ($\sim 30\%$). Finally, a redshift-dependence given by $M_R^\star(z) = M_R^\star(0) + 5\log(1+z)$ was assumed to account for galaxy evolution in the clusters. The combination of all these effects would predict a surface density of cluster galaxies which is 7% less at $z = 0.3$, compared to $z = 0.23$, for a fixed cluster richness. Even this small difference would be erased by a slight decrease in the assumed values of the slopes $\alpha^\star$ and a. A faint-end slope of the luminosity function of $\alpha^\star = -1.1$ would be sufficient to remove the predicted difference in galaxy surface density at the two different redshifts. Based on *Hubble Space Telescope* (HST) WFPC2 imaging of the galaxy cluster A2218 (which is similar to the clusters studied here in terms of optical richness, lensing mass and X-ray properties), Pracy et al. (2004) find that the cluster core shows a relative depletion of dwarf galaxies, leading to a radial profile of faint galaxies which is significantly shallower than the SIS prediction. For the "intermediate" dwarf population ($-18 < M_{\rm F606W} < -15$, similar to the range in absolute magnitude of cluster galaxies in our faint galaxy catalogs), these authors find a radial distribution with a slope $a = -0.63 \pm 0.09$. Assuming a similar slope for the radial distribution of the faint cluster galaxies in our catalogs would also remove the predicted difference between the two curves in Figure 1. Based on this figure, and the above discussion, we conclude that we are probably justified in ignoring the redshift-dependence in our cluster galaxy contamination correction.

The level of cluster galaxy contamination for individual clusters will generally differ from the mean level calculated above, as there will be significant cluster-to-cluster variations in the abundances of cluster dwarf galaxies. Based on the sample of clusters observed with the UH8K camera, the scatter in dwarf galaxy richness was estimated to be $\sim 50\%$ (this estimate also includes variations in the field galaxy density caused by uncorrelated large-scale structures along the line of sight, and hence the true scatter in dwarf galaxy richness of the clusters is somewhat overestimated). By employing the mean contamination correction calculated above rather than an estimate appropriate for each cluster, we introduce an additional scatter of up to 20% in our mass estimates. This additional scatter is not included in the uncertainties of the tabulated mass measurements in Table 1, but is considered further in Section 3.2.

Eight of the clusters in our sample were also included in the combined strong and weak gravitational lensing study of S05, based on observations of a sample of 10 X-ray luminous galaxy clusters at $z \sim 0.2$ using HST WFPC2. These authors estimated the projected cluster mass within a cluster-centric radius of $250h^{-1}$ kpc, assuming an Einstein-de Sitter ($\Omega_m = 1$, $\Omega_\Lambda = 0$) cosmology. Figure 2 shows a comparison of the mass values listed by S05 with our cluster mass estimates, using the best-fit NFW model to derive projected cluster masses, assuming the same cosmology as S05. These authors assumed a spatially constant contamination of 20% cluster galaxies in their background galaxy catalogs at radii $< 2'$, while we find an average contamination of 30% for our data at these radii. Hence, for the plot in Figure 2 we have adjusted our radially dependent contamination correction such that the average contamination at small radii is consistent with that assumed by S05. We find that our cluster mass estimates are generally consistent with those of S05, although with a tendency for higher masses (by about 30%).

2.2. *X-ray data*

For clusters in the weak lensing data set, we compiled a list of corresponding X-ray temperatures from the literature. For many of these clusters, their global temperature, or even a temperature map, has been determined using data

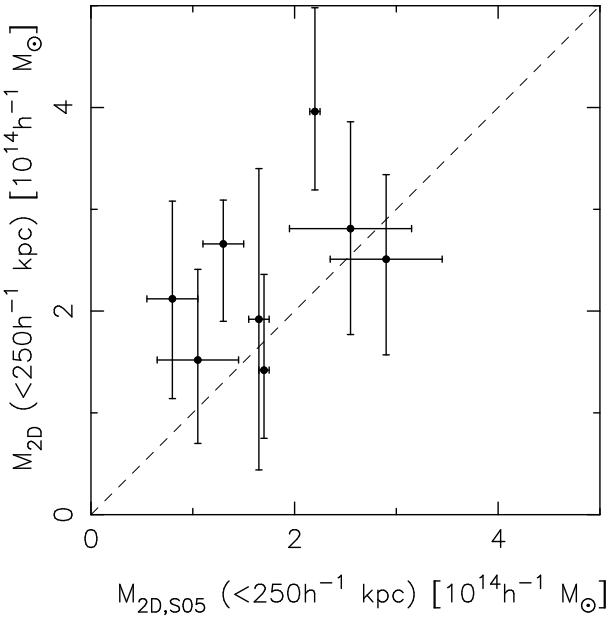

FIG. 2.— Comparison with estimates of the projected mass within $250h^{-1}$ kpc published by S05. The lensing masses in this plot are given for the cosmological model assumed by S05, and our estimate of the degree of galaxy cluster contamination was also adjusted to match the contamination assumed by S05 (see text for details).

from *Chandra* and/or XMM-Newton. However, these temperatures constitute a rather heterogeneous sample, for which the systematics are not well established. Consequently, X-ray temperatures were primarily drawn from the samples of Ota & Mitsuda (2004), Allen (2000) and White (2000), each providing a homogeneous measure of the global cluster temperature (i.e., temperature measured within a cluster-centric distance close to r_{500c}) for a large fraction of the clusters in the weak lensing sample. All these authors derived temperatures based on analysis of ASCA spectra. For two clusters not in either of the samples mentioned above we extracted published temperatures from other sources.

Specifically, from the works of Ota & Mitsuda (2004) and Allen (2000) we extracted temperatures estimated by these authors by fitting an isothermal plasma model with the Galactic absorbing column density as a free parameter. The temperatures taken from White (2000) were derived by fitting an isothermal plasma model with the nominal Galactic absorbing column density fixed, but since only energies above 1 keV are used in the White (2000) spectral fitting the fixed column density should not introduce systematic effects relative to the temperatures from the Ota & Mitsuda (2004) and the Allen (2000) samples. For the remaining two clusters we extracted published temperatures obtained in a similar way (see Table 1).

For the clusters in two or more samples, their derived temperatures agree within the uncertainties, and for any cluster the derived temperatures differ by less than 20% between samples. Also, the mean of temperature differences between any two of the samples by Ota & Mitsuda (2004), Allen (2000), and White (2000) is less than 3%, indicating the low level of systematic temperature variance between different analyses.

Although the isothermal plasma model has proven too simplistic for nearby clusters, the global cluster temperature is straightforward to derive from observations as well as simulations, enabling a rather direct comparison between observations and theory. Furthermore, for the majority of distant ($z \gtrsim 0.5$) clusters only global isothermal temperatures can be obtained in the foreseeable future. Hence, we refrain from going into the detailed spatial and spectral modeling of the intracluster gas. The effects of cluster dynamics, "cooling cores", non-sphericity etc. generally affects the global temperatures only at the 10%-20% level (e.g., Evrard, Metzler, & Navarro 1996; White 2000; Smith et al. 2005).

3. RESULTS

From the virial relation

$$M \propto \langle v^2 \rangle r \propto Tr, \tag{3}$$

between cluster mass, M, inside radius r, galaxy velocity, v, and gas temperature, T, combined with the definition of mass within an over-density of 500 times the critical density

$$M_{500c} \propto r^3_{500c}\rho_c(z) \propto r^3_{500c}E^2(z)\rho_c(0) \propto r^3_{500c}E^2(z), \tag{4}$$

where the term $E^2(z) = \rho_c(z)/\rho_c(0)$ describes the evolution of the over-density for a given cosmology, the mass–temperature relation is obtained as

$$E(z)M_{500c} \propto T^{3/2}. \tag{5}$$

In this study, we have measured M_{500c}, relating to $M_{\rm vir}$ through $M_{\rm vir} = 1.65M_{500c}$ for the average cluster redshift with our chosen NFW model. We take into account that the slope may deviate from the simple theoretical expectation $\alpha = 3/2$ and normalize the relation at 8 keV since our sample is dominated by massive clusters. Hence, mass–temperature relations were obtained by fitting the data in Table 1 using the BCES($X_2|X_1$) estimator of Akritas & Bershady (1996) to the following parameterization of the mass–temperature relation

$$E(z)M_{500c} = M_{500c,8\rm keV}(T/8\rm keV)^{\alpha}. \tag{6}$$

The redshift-dependent factor, $E(z)$, contained in eq.6 must be calculated individually for each cluster, as this would otherwise produce an artificial 15% variation in mass over the redshift range spanned by our cluster sample. In effect, the normalization of the relation refers to the present epoch ($z = 0$).

The fitting procedure of Akritas & Bershady (1996) takes uncertainties in temperatures as well as in weak lensing masses into account, and makes no assumptions about the intrinsic scatter of both quantities. Results from fitting subsamples as well as the full sample are presented in Table 2 and Figure 3.

For the full data set (for those clusters with temperature from more than one sample the temperature was taken in prioritized order from Ota & Mitsuda (2004), Allen (2000), and White (2000)) we find the following normalization of the mass–temperature relation at 8 keV $M_{500c,8\rm keV} = (8.7 \pm 1.6) \times 10^{14}h^{-1}M_{\odot}$ and a slope of $\alpha = 0.49 \pm 0.80$. It is evident that the slope of the mass–temperature relation is not well-determined since our data only span a modest range at the high mass/high temperature end of the cluster distribution. In fact, it is not obvious that there is a tight mass–temperature relation at the high temperature end probed here.

3.1. *Normalization of the mass–temperature relation and* σ_8

The concentration of clusters around 6 – 8 keV enables a robust measurement of the normalization of the mass–temperature relation at the high–mass end. Even though the

TABLE 1
Weak lensing masses and X-ray temperatures

Cluster	z_{cl} [a]	M_{500c} ($10^{14}\,h^{-1}M_\odot$)	r_{fit}/r_{500c}	kT (Ota & Mitsuda) (keV)	kT (Allen) (keV)	kT (White) (keV)	kT (other)[b] (keV)
A68	0.255	$21.37^{+6.79}_{-7.20}$	0.30	$6.93^{+0.63}_{-0.59}$	...	...	...
A115	0.197	$2.42^{+2.34}_{-1.84}$	0.50	$5.83^{+0.47}_{-0.30}$	...	...	...
A209	0.206	$7.54^{+4.24}_{-3.87}$	1.62	...	...	...	$7.10^{+0.40}_{-0.40}$
A267	0.230	$8.79^{+2.87}_{-3.53}$	1.32	$5.51^{+0.44}_{-0.41}$	...	...	...
A520	0.203	$8.67^{+3.36}_{-2.60}$	1.20	...	$7.94^{+0.96}_{-0.90}$	...	...
A586	0.171	$25.27^{+7.01}_{-8.11}$	0.21	$6.96^{+0.99}_{-0.83}$	$7.02^{+0.94}_{-0.80}$	$6.06^{+0.64}_{-0.52}$	...
A611	0.288	$3.83^{+2.99}_{-2.79}$	0.59	...	...	$6.85^{+0.48}_{-0.46}$	...
A665	0.182	$5.40^{+3.40}_{-3.07}$	0.36	$6.96^{+0.28}_{-0.27}$	$8.12^{+0.62}_{-0.54}$	$7.73^{+0.41}_{-0.35}$	...
A697	0.282	$12.18^{+4.97}_{-4.89}$	0.39	$8.19^{+0.62}_{-0.60}$	...	$8.60^{+0.50}_{-0.49}$	...
A773	0.217	$13.09^{+4.79}_{-6.15}$	0.30	$8.07^{+0.70}_{-0.66}$	$8.29^{+0.73}_{-0.64}$	$8.63^{+0.68}_{-0.67}$	...
A959	0.285	$9.33^{+3.50}_{-3.05}$	1.45	$5.24^{+0.89}_{-0.73}$	...	...	...
A963	0.206	$4.42^{+4.27}_{-3.46}$	1.51	$6.83^{+0.51}_{-0.51}$	$6.13^{+0.45}_{-0.30}$	$6.08^{+0.43}_{-0.33}$	...
A1576	0.299	$8.62^{+3.40}_{-2.54}$	1.58	...	...	$6.57^{+0.56}_{-0.54}$	...
A1682	0.226	$2.24^{+1.9}_{-1.33}$	0.55	$6.42^{+0.63}_{-0.60}$	...	$7.24^{+0.68}_{-0.59}$	...
A1722	0.325	$2.70^{+2.14}_{-1.58}$	2.58	$5.81^{+0.59}_{-0.39}$	...	...	...
A1758N	0.280	$20.37^{+6.37}_{-6.65}$	0.33	$6.88^{+0.86}_{-0.75}$	...	...	...
A1763	0.228	$4.90^{+2.42}_{-3.07}$	0.45	$8.11^{+0.66}_{-0.63}$	...	$7.30^{+0.46}_{-0.38}$	...
A1835	0.253	$8.42^{+4.41}_{-3.33}$	0.39	$7.42^{+0.61}_{-0.43}$	$7.33^{+0.35}_{-0.30}$	$7.88^{+0.49}_{-0.46}$	...
A1914	0.171	$2.62^{+2.03}_{-1.93}$	0.44	...	...	$10.53^{+0.51}_{-0.50}$	...
A1995	0.320	$23.69^{+6.88}_{-6.13}$	1.23	$9.06^{+1.77}_{-1.32}$	...	$7.57^{+1.07}_{-0.76}$	...
A2104	0.153	$14.14^{+5.34}_{-5.55}$	0.23	$7.66^{+0.49}_{-0.43}$	...	$9.12^{+0.48}_{-0.46}$	...
A2111	0.229	$3.84^{+1.80}_{-2.14}$	0.47	$6.94^{+0.76}_{-0.67}$	...	...	...
A2204	0.152	$7.86^{+5.28}_{-4.57}$	0.27	$6.68^{+0.28}_{-0.27}$	$6.23^{+0.30}_{-0.28}$	$6.99^{+0.24}_{-0.23}$	...
A2219	0.228	$4.72^{+2.35}_{-2.94}$	0.45	...	$9.46^{+0.63}_{-0.57}$	$9.52^{+0.55}_{-0.40}$	...
A2261	0.224	$11.52^{+5.40}_{-5.97}$	0.32	$6.56^{+0.49}_{-0.48}$	$6.64^{+0.51}_{-0.46}$	$7.49^{+0.57}_{-0.43}$	...
MS1455+22	0.258	$3.21^{+2.19}_{-1.78}$	0.58	...	$4.33^{+0.27}_{-0.25}$	$4.83^{+0.22}_{-0.21}$	...
RX J1532.9+3021	0.345	$13.86^{+5.93}_{-5.64}$	0.44	$4.91^{+0.29}_{-0.30}$	...	...	...
RX J1720.1+2638	0.164	$3.28^{+2.65}_{-2.53}$	0.39	...	...	...	$5.60^{+0.50}_{-0.50}$
RX J2129.6+0005	0.235	$8.35^{+4.62}_{-4.87}$	0.38	$5.72^{+0.38}_{-0.30}$	...	...	...
Zw3146	0.291	$7.57^{+4.13}_{-3.25}$	0.47	...	$6.80^{+0.38}_{-0.36}$	$5.89^{+0.30}_{-0.22}$	...

[a] — See Ebeling et al. (1996; 1998) for references to redshift measurements.[b] — kT value for A209 from P.B. Marty (private communication); kT value for RXJ1720.1+2638 from Mazzotta et al. (2001).

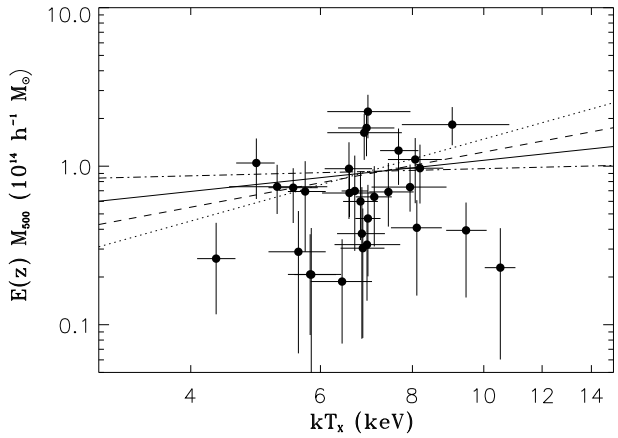

FIG. 3.— Weak lensing mass estimates and X-ray temperatures with BCES($X_2|X_1$) regression lines for different subsamples. The full line is the fit to the full sample, defined as described in the text; the dotted line is the fit to the Ota & Mitsuda (2004) sample; the dashed line is the fit to the Allen (2000) sample; and the dot–dashed line is the fit to the White (2000) sample.

slope of the mass–temperature relation varies substantially between the three X-ray sub-samples (Ota & Mitsuda 2004; Allen 2000; White 2000) the best fit normalizations agree within their statistical uncertainty. We note that for all fits, the four different regressions of Akritas & Bershady (1996) all result in normalizations within 20%.

The strongest constraints on the mass–temperature relation normalization are obtained by taking advantage of previous studies of massive clusters (Finoguenov, Reiprich, & Böhringer 2001; Allen, Schmidt, & Fabian 2001; Arnaud, Pointecouteau, & Pratt 2005), showing that the mass–temperature relation slope is close to $\alpha = 3/2$ as expected from simple gravitational collapse models (Kaiser 1986). Hence, in order to express the normalization of the mass–temperature relation in terms of the characteristic temperature $T_\star = 8\mathrm{keV}\,(1.65 M_{500c,8\mathrm{keV}})^{-1/\alpha}$ (Pierpaoli, Borgani, Scott, & White 2003) we assume $\alpha = 3/2$ (with a representative uncertainty of 10%, e.g. Finoguenov, Reiprich, & Böhringer 2001). As is custom for quoting $T_\star$ values we adopt the redshift dependence factor $F(z) = \left(\Delta_c E^2\right)^{-1/2}\left[1 - 2\frac{\Omega_\Lambda(z)}{\Delta_c}\right]^{-3/2}$ (Pierpaoli, Borgani, Scott, & White 2003) where Δ_c is the mean overdensity inside the virial radius in units of the critical density at the relevant redshift ($F(z)$ and $E(z)$ differs by 7% at $z = 0.23$).

We find $T_\star = 1.28 \pm 0.20$ for our full sample and results from calculations of $T_\star$ based on various subsamples are listed in Table 3. From the σ_8 - $T_\star$ relation plotted by

Pierpaoli, Borgani, Scott, & White (2003) in their Figure 2, we find $\sigma_8 = 0.88 \pm 0.09$, based on our full sample. We note that this relation is valid only for an intrinsic scatter in temperature of $\lesssim 10\%$ around the mean mass–temperature relation. A larger intrinsic scatter will imply a lower value of σ_8. We provide our constraints on the intrinsic scatter below.

3.2. *Scatter in the mass–temperature relation*

The squared scatter in lensing mass, M_{500c}, around the best fit, $(\sigma_M^{tot})^2 = \langle(\frac{M^i_{500c}-M^{fit}_{500c}}{M^i_{500c}})^2\rangle$, is the sum of the squared measurement error, the squared intrinsic scatter, and the squared systematic errors $(\sigma_M^{tot})^2 = (\sigma_M^{err})^2 + (\sigma_M^{i})^2 + (\sigma_M^{sys})^2$. The main systematic errors in the lensing mass (see Section 2.1) arise from extrapolating the assumed NFW mass profile out to r_{500c} (due to cluster-to-cluster variations in the assumed concentration parameter c_{vir}) and from the separation of cluster/background galaxies (due to cluster-to-cluster richness variations). Each of these introduces a scatter of 20% in the lensing mass, hence $\sigma_M^{sys} = 0.28$. For the full sample we find $\sigma_M^{tot} = 0.94$ which is larger than expected from the mean lensing mass error, $\sigma_M^{err} = 0.52$ and the systematic errors, indicating either a sizable intrinsic scatter in mass or that the measurement/systematic errors are severely under-estimated.

Accounting for errors in both mass and temperature, we find an intrinsic scatter in $T_\star$ of $0.25^{+0.28}_{-0.25}$. There is a 70% probability that the scatter in temperature is larger than 10%, favoring somewhat lower values of σ_8 than quoted above. However, most of the scatter is caused by the low mass clusters.

3.3. *Relaxed vs. non-relaxed clusters*

We looked into whether relaxed clusters and non-relaxed clusters have the same normalization of the mass–temperature relation. Our "relaxed" cluster sample consists of A586, A963, A1835, A1995, A2204, A2261, RXJ1720, and RXJ1532. These are clusters with "spherical" optical and X-ray morphology, and no known cluster-scale dynamic disturbances. For the relaxed clusters we find a normalization of the mass–temperature relation of $M_{500c,8keV,relax} = (17.3 \pm 3.7) \times 10^{14} h^{-1} M_\odot$ while the normalization for the non-relaxed clusters is $M_{500c,8keV,nonrelax} = (7.6 \pm 1.5) \times 10^{14} h^{-1} M_\odot$ (see Figure 4). The higher normalization of relaxed clusters is supported by the fact that the mean mass of relaxed clusters is a factor 1.5 larger than the mean mass of "non-relaxed" clusters, although the relaxed and the non-relaxed clusters span roughly the same temperature range.

The scatter in mass for the relaxed sample ($\sigma_M^{tot} = 0.77$) is similar to the scatter for the non-relaxed sample ($\sigma_M^{tot} = 0.88$). The mean error for both samples is $\sigma_M^{err} = 0.57$. Either relaxed clusters spread as much around their mass–temperature relation as clusters in general, or we have used a poor definition of "relaxed" clusters. However, the fact that the normalization of the mass–temperature relation for relaxed clusters is higher than for non-relaxed clusters indicates that there is a physical difference between the two sub-samples. From the present study, it thus seems that relaxed clusters do not form a tighter mass–temperature relation than clusters in general.

For a given mass, non-relaxed clusters are found to be $\sim 75 \pm 40\%$ hotter than relaxed clusters. Since we consider global, isothermal temperatures, the presence of "cooling cores" in relaxed clusters will result in a lower global temperature than the virial temperature. However, this effect is at the 10%-20% level (e.g., Smith et al. 2003a; O'Hara et al. 2006) so this cannot alone explain the temperature difference between relaxed and non-relaxed clusters. Based on the mass–temperature relation from 10 clusters (3 of which are considered relaxed), S05 also find that non-relaxed clusters are hotter than relaxed clusters. An objective classification of the degree of relaxation for a sizeable cluster sample is required for further quantifying the size of this effect.

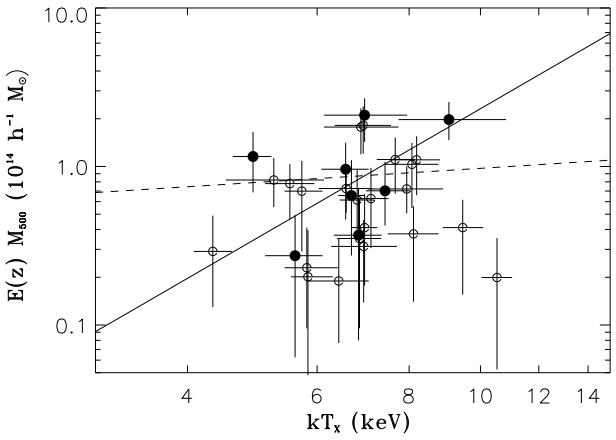

FIG. 4.— Weak lensing mass estimates and X-ray temperatures with BCES($X_2|X_1$) regressions for "relaxed" clusters (filled symbols, full line) and "non-relaxed" clusters (open symbols, dashed line).

TABLE 2
BEST-FIT MASS-TEMPERATURE RELATION (ARBITRARY SLOPE)

$M_{500c,8keV}$ ($10^{14} h^{-1} M_\odot$)	α	Sample
12.0 ± 2.4	1.30 ± 0.97	Ota & Mitsuda (2004)
9.5 ± 1.9	0.87 ± 0.78	Allen (2000)
8.1 ± 1.5	0.11 ± 0.98	White (2000)
8.7 ± 1.6	0.49 ± 0.80	All
17.3 ± 3.7	2.69 ± 1.30	"Relaxed"
7.6 ± 1.5	0.29 ± 0.76	"Non-relaxed"

TABLE 3
BEST-FIT MASS-TEMPERATURE RELATION (FIXED SLOPE)

$T_\star$	α	Sample
1.04 ± 0.18	3/2	Ota & Mitsuda (2004)
1.22 ± 0.21	3/2	Allen (2000)
1.35 ± 0.21	3/2	White (2000)
1.28 ± 0.20	3/2	All
0.82 ± 0.14	3/2	"Relaxed"
1.42 ± 0.22	3/2	"Non-relaxed"

NOTE. — The uncertainty in $T_\star$ from α has been taken to be 10%.

4. DISCUSSION

Based on the hitherto largest sample of X-ray luminous clusters with measured lensing masses, we derive a normalization of the mass–temperature relation at the high mass end, $M_{500c,8keV} = (8.7 \pm 1.6)\, h^{-1}\, 10^{14} M_\odot$. This value is higher than the lensing based mass–temperature normalization of S05, based on a smaller cluster sample, but is consistent with

TABLE 4
NORMALIZATIONS OF THE MASS-TEMPERATURE RELATION

Method	$\langle z \rangle$	$M_{500c,8keV}$	Slope	Reference
X-rays	0.09	6.00 ± 0.35	Fitted	Arnaud, Pointecouteau, & Pratt (2005)
	0.09	6.07 ± 0.46	Fitted	Vikhlinin et al. (2006)
Lensing	0.23	6.65 ± 0.52	Fixed	S05
	0.23	8.67 ± 1.57	Fitted	This study
Simulations	0.04	8.09 ± 0.48	Fixed	Evrard, Metzler, & Navarro (1996)
	0.00	6.82 ± 0.76	Fitted	Borgani et al. (2004)

NOTE. — Included here are some recent studies with a quoted normalization of the $M_{500c} - T$–relation, scaled to $M_{500c,8keV}$, i.e., the mass contained within r_{500c} of a cluster with $kT = 8$keV, with errors propagated, and assuming $h = 1$. The listed normalization has been scaled to a common redshift of $z = 0$. The normalization of S05, which was determined within a fixed physical radius of $250h^{-1}$ kpc in an Einstein-de Sitter universe, has been scaled to M_{500c} for our adopted cosmology, making the same assumptions about an NFW-type mass profile as we have made for our own data. For each study, we indicate whether the slope of the relation was calculated from a fit to the data, or whether the slope was fixed at the theoretically expected value, $\alpha = 3/2$.

this within 1σ errors; see Table 4. Mass–temperature relations with masses determined from X-ray data tend to have a lower normalization than lensing based relations, and they are only marginally consistent with our normalization. This is also the case for the two recent studies of Vikhlinin et al. (2006) and Arnaud, Pointecouteau, & Pratt (2005) based on smaller samples of lower mass (and hence cooler) clusters. Vikhlinin et al. (2006) measured cluster masses inside r_{500c} from X-ray observations of a sample of 13 low redshift clusters with a median temperature of 5.0 keV while Arnaud, Pointecouteau, & Pratt (2005) determined the normalization from X-ray derived masses of 10 nearby clusters with a mean temperature of 4.8 keV. The two studies agree on the same normalization, higher than previous X-ray mass based studies, but there still seems to be a $\sim$ 20% discrepancy between X-ray and lensing derived mass–temperature relations.

We note, however, that the lensing based and X-ray based normalizations are made at different redshifts, and that this discrepancy would vanish if the redshift-dependence predicted by the self-similar collapse model in equation 5 were neglected. Given the heterogeneous nature of these data sets, any claim of significant departures from self-similarity would be premature, but this clearly provides an interesting avenue for future research, involving even larger cluster samples spanning a wider interval in redshift.

We confirm the result of Smith et al. (2005) that non-relaxed clusters are on average significantly hotter than relaxed clusters. This is qualitatively consistent with N-body/hydrodynamical cluster simulations which show that major mergers can temporarily boost the X-ray luminosities and temperatures well above their equilibrium values (e.g. Randall et al. 2002).

In contrast to several previous (mainly X-ray mass based) published mass–temperature relations, the normalization derived in this study is in good agreement with the normalization derived from numerical simulations. However, the accuracy of the normalization is not good enough to discriminate between simulations including different physical processes. Our results show that X-ray based measurements of the cluster abundances, after reducing the major systematic uncertainties associated with the mass–temperature normalization, give an amplitude of mass fluctuations on cluster scales that is consistent with other methods. This lends additional support to the "concordance model" cosmology, and lends credence to the basic assumptions of Gaussian density fluctuations. Our determination of $\sigma_8 = 0.88 \pm 0.09$ is higher than most σ_8 determinations from cluster data (for a compilation of these, see e.g., Henry 2004). However, our finding is consistent with the value derived from weak gravitational lensing in the combined Deep and Wide CFHT Legacy Survey ($\sigma_8 = 0.86 \pm 0.05$; Semboloni et al. 2005) based on the halo model of density fluctuations (Smith et al. 2003b). It is also consistent with the CMB+2dFGRS+Ly$_\alpha$ forest result ($\sigma_8 = 0.84 \pm 0.04$) of Spergel et al. (2003), with the joint CMB + weak lensing analysis of Contaldi, Hoekstra, & Lewis (2003), which gave $\sigma_8 = 0.89 \pm 0.05$, and with CMB analyses (Bond et al. 2005) yielding $\sigma_8 \approx 0.9$. However, the more recent 3-year WMAP results (Spergel et al. 2006) give a significantly lower value of σ_8, and also a preference for a value of Ω_m lower than 0.3. Also, results from the recent 100 square degree weak lensing survey (Benjamin et al. 2007) favor a lower value of $\sigma_8 = 0.74 \pm 0.06$ for $\Omega_m = 0.3$. We note that our quoted value of σ_8 is based on the assumption that the intrinsic scatter about the mass–temperature relation is $\lesssim$ 10%, and that our σ_8 estimate will be biased high if the true scatter significantly exceeds this value (Pierpaoli, Borgani, Scott, & White 2003).

The limiting factor of our measurement of the normalization of the mass–temperature relation is the magnitude of the measurement errors (dominating the systematic errors, estimated to be $\sim$ 30%). In order for the mass–temperature relation to be a competitive route for constraining cosmological parameters and to discriminate between simulations with different input physics, the normalization must be measured to better than $\sim$ 10% accuracy. However, there are good prospects for improving on these results in the near future. Firstly, the superior spectro-imaging capabilities of *Chandra*

and XMM-Newton will allow the construction of large, homogeneous cluster temperature samples. A comparison to tailored simulations with realistic physics, analyzed in the same way as observations, will advance our understanding of systematics and the link between the mass–temperature relation and structure formation (C.B. Hededal et al. 2007, in preparation). Secondly, more accurate weak lensing-based mass measurements of a larger sample of clusters are feasible as large mosaic CCD cameras that can probe intermediate-redshift clusters beyond their virial radii are now common, and the cluster sample could easily be doubled from a similar survey in the Southern celestial hemisphere.

Finally, we note that a more direct measurement of σ_8 from weak lensing by clusters is possible, provided that weak lensing mass estimates are available for a large, well-defined, volume-limited cluster sample. This makes it feasible to calculate the cluster mass function directly from the lensing masses, rather than indirectly via the X-ray temperature function (Dahle 2006). Since mass estimates based on baryonic tracers of the total cluster mass only enters indirectly as a selection criterion (e.g., clusters selected based on X-ray luminosity above a certain threshold), the method is less susceptible to systematic and random errors, as it does not require an accurate characterization of the scatter around the mean mass–temperature relation.

We thank Per B. Lilje and Jens Hjorth for valuable comments on a draft version of this paper. We also thank the anonymous referee for comments and suggestions that improved the presentation of our results. KP acknowledges support from the Danish National Research Council, the Carlsberg foundation, and Instrument Center for Danish Astrophysics. The Dark Cosmology Centre is funded by the Danish National Research Foundation. HD acknowledges support from the Research Council of Norway and travel support from NORDITA.

REFERENCES

Abell, G. O. 1958, ApJS, 3, 211
Abell, G. O., Corwin, H. G., & Olowin, R. P. 1989, ApJS, 70, 1
Akritas, M. G. & Bershady, M. A. 1996, ApJ, 470, 706
Allen, S. W. 2000, MNRAS, 315, 269
Allen, S. W., Schmidt, R. W., & Fabian, A. C. 2001, MNRAS, 328, L37
Arnaud, M., Pointecouteau, E., & Pratt, G. W. 2005, A&A, 441, 893
Benjamin, J., et al. ArXiv Astrophysics e-prints, arXiv:astro-ph/0703570
Bond, J.R., et al. 2005, ApJ, 626, 12
Borgani, S., Girardi, M., Carlberg, R. G., Yee, H. K. C., & Ellingson, E. 1999, ApJ, 527, 561
Borgani, S. et al. 2004, MNRAS, 348, 1078
Böhringer, H. et al. 2003, ApJ, 566, 93
Briel, U. G. & Henry, J. P. 1993, A&A, 278, 379
Bullock, J. S., Kolatt, T. S., Sigad, Y., Somerville, R. S., Kravtsov, A. V., Klypin, A. A., Primack, J. R., & Dekel, A. 2001, MNRAS, 321, 559
Carlberg, R. G., Morris, S. L., Yee, H. K. C., & Ellingson, E. 1997, ApJ, 479, L19
Contaldi, C. R., Hoekstra, H., & Lewis, A. 2003, Physical Review Letters, 90, 221303
Clowe, D., De Lucia, G., & King, L. 2004, MNRAS, 350, 1038
Dahle, H., Kaiser, N., Irgens, R. J., Lilje, P. B., & Maddox, S. J. 2002, ApJS, 139, 313
Dahle, H. 2006, ApJ, 653, 954
de Putter, R., & White, M. 2005, New Astronomy, 10, 676
Ebeling, H., Voges, W., Bohringer, H., Edge, A. C., Huchra, J. P., & Briel, U. G. 1996, MNRAS, 281, 799
Ebeling, H., Edge, A. C., Bohringer, H., Allen, S. W., Crawford, C. S., Fabian, A. C., Voges, W., & Huchra, J. P. 1998, MNRAS, 301, 881
Ebeling, H., Edge, A. C., Allen, S. W., Crawford, C. S., Fabian, A. C., & Huchra, J. P. 2000, MNRAS, 318, 333
Eke, V. R., Navarro, J. F., & Frenk, C. S. 1998, ApJ, 503, 569
Evrard, A. E., Metzler, C. A., & Navarro, J. F. 1996, ApJ, 469, 494
Finoguenov, A., Reiprich, T. H., & Böhringer, H. 2001, A&A, 368, 749
Frenk, C. S., White, S. D. M., Efstathiou, G., & Davis, M. 1990, ApJ, 351, 10
Henry, J. P. 2004, ApJ, 609, 603
Heymans, C., et al. 2006, MNRAS,368, 1323
Hjorth, J., Oukbir, J., & van Kampen, E. 1998, MNRAS, 298, L1
Hoekstra, H. 2001, A&A, 370, 743
Huterer, D. & White, M. 2002, ApJ, 578, L95
Kaiser, N. 1986, MNRAS, 222, 323
Mazzotta, P., Markevitch, M., Vikhlinin, A., Forman, W. R., David, L. P., & VanSpeybroeck, L. 2001, ApJ, 555, 205
Metzler, C. A., White, M., & Loken, C. 2001, ApJ, 547, 560
Navarro, J. F., Frenk, C. S., & White, S. D. M. 1997, ApJ, 490, 493
Ota, N. & Mitsuda, K. 2004, A&A, 428, 757
O'Hara, T. B., Mohr, J. J., Bialek, J. J., & Evrard, A. E. 2006, ApJ, 639, 64
Pen, U. 1998, ApJ, 498, 60
Pierpaoli, E., Scott, D., & White, M. 2001, MNRAS, 325, 77
Pierpaoli, E., Borgani, S., Scott, D., & White, M. 2003, MNRAS, 342, 163
Pracy, M. B., De Propris, R., Driver, S. P., Couch, W. J., & Nulsen, P. E. J. 2004, MNRAS, 352, 1135
Randall, S. W., Sarazin, C. L., & Ricker, P. M. 2002, ApJ, 577, 579
Reiprich, T. H. & Böhringer, H. 2002, ApJ, 567, 716
Rosati, P., Borgani, S., Norman, C. 2002, ARA&A, 40, 539
Sanderson, A. J. R., Ponman, T. J., Finoguenov, A., Lloyd-Davies, E. J., Markevitch, M., Reiprich, T. H. & Böhringer, H. 2002, MNRAS, 340, 989
Schechter, P. 1976, ApJ, 203, 297
Seljak, U. 2002, MNRAS, 337, 769
Semboloni, E., et al. 2006, A&A, 452, 51
Smith, G. P., Edge, A. C., Eke, V. R., Nichol, R. C., Smail, I., & Kneib, J. 2003a, ApJ, 590, L79
Smith, R. E., et al. 2003b, MNRAS, 341, 1311
Smith, G. P., Kneib, J.-P., Smail, I., Mazzotta, P., Ebeling, H., & Czoske, O. 2005, MNRAS, 359, 417
Spergel, D. N., et al. 2003, ApJS, 148, 175
Spergel, D. N., et al. 2006, ArXiv Astrophysics e-prints, arXiv:astro-ph/0603449
Stanek, R., Evrard, A. E., Böhringer, H., Schuecker, P., & Nord, B. 2006, ApJ, 648, 956
Trümper, J. 1993, Science, 260, 1769
Vikhlinin, A. et al. 2006, ApJ, 640, 691
White, D. A. 2000, MNRAS, 312, 663